

# Collapse Prevention seismic performance assessment of new buckling-restrained braced frames using ASCE 41

Matthew S. Speicher\*, John L. Harris III

National Institute of Standards and Technology, 100 Bureau Drive, Gaithersburg, MD 20899, USA



## ARTICLE INFO

### Keywords:

Performance-based seismic design  
Buckling-restrained braced frame  
Performance assessment  
ASCE 41  
Steel structures

## ABSTRACT

This paper presents the results of a seismic performance assessment using ASCE 41-13 for six buckling-restrained braced frames (BRBFs) designed in accordance with the 2012 *International Building Code*. The correlation between ASCE 7-10 and ASCE 41-13 is investigated to compare the seismic performance anticipated by the two standards. Three archetype buildings (4-, 8-, and 16-story) with BRBFs along one principal direction are designed for seismic effects: (1) once using the equivalent lateral force (ELF) procedure and (2) a second time using the response spectrum analysis (RSA) procedure. Performance assessments are conducted using four analysis procedures, static and dynamic analyses performed under both linear and nonlinear analysis regimes. Linear analysis results indicate minor performance deficiencies in the columns and the braces. Surprisingly, the nonlinear analysis results indicate more performance deficiencies in the braces, which is opposite of the general expectation that a more sophisticated analysis would yield a less conservative result. The contributing factors to the performance deficiencies are investigated. Recommendations are made on how to alter the performance outcome such as using alternative ground motion selection approaches (e.g., conditional mean spectrum) and having acceptance criteria based on cumulative ductility demands.

## 1. Introduction

The popularity of performance-based seismic design (PBSD) as a way to directly achieve a suitable seismic performance level has created the need for more understanding regarding how current PBSD methodologies compare to their established prescriptive counterparts. ASCE/SEI 7-10 [1] (hereafter ASCE 7) allows the use of PBSD for new buildings. However, with no methodology specified to achieve the anticipated performance objective, practitioners often apply the PBSD techniques developed for evaluating existing buildings in ASCE/SEI 41-13 [2] (hereafter ASCE 41). Potential problems arise because ASCE 41 contains a number of presumably conservative assumptions to account for typically large uncertainties in evaluating existing buildings. Limited investigation into the correlation between the performance objectives of the two standards has been performed.

A NIST report titled *Research Required to Support Full Implementation of Performance-Based Seismic Design* listed benchmarking ASCE 41 procedures as the top practitioner-oriented need because of perceived conservatism and known inconsistencies between PBSD and prescriptive design procedures [3]. Some researchers have investigated the ASCE 41 performance of ASCE 7-designed buildings. Adams [4] investigated the behavior of a 6-story special concentrically braced frame

designed using ASCE 7 and found that ASCE 41 procedures give widely varying results, with the nonlinear procedures indicating more performance deficiencies than the linear procedures. Burkholder [5] similarly used ASCE 41 to investigate the behavior of a 6-story buckling-restrained braced frame (BRBF) designed using ASCE 7. However, ASCE 41 had yet to include acceptance criteria for buckling-restrained braces (BRBs), therefore that study used acceptance criteria for conventional braces in tension for the linear procedures and acceptance criteria derived from experimental BRB data for the nonlinear procedures. Burkholder's results indicated the frames passed both the linear and nonlinear procedures. In contrast, Speicher and Harris [6,7] investigated the behavior of a suite of braced frames designed with ASCE 7 and found that ASCE 41 indicated widely varying levels of performance. Given that some code jurisdictions are allowing the use of ASCE 41 as the basis for new building design and that BRBF provisions were added in ASCE 41-13, further investigation is warranted. The basic question addressed in this paper is whether the standards for designing new buildings and assessing existing buildings provide consistent levels of performance.

This paper presents the results of a structural seismic performance assessment using ASCE 41 for six BRBFs located in a region of high seismicity. Three BRBFs are designed using both the equivalent lateral

\* Corresponding author.

E-mail addresses: [matthew.speicher@nist.gov](mailto:matthew.speicher@nist.gov) (M.S. Speicher), [john.harris@nist.gov](mailto:john.harris@nist.gov) (J.L. Harris).

force (ELF) and response spectrum analysis (RSA) procedures to provide two different levels of seismic force-resisting system (SFRS) strength. Performance assessments are conducted using the linear static and dynamic procedures and the nonlinear static and dynamic procedures as prescribed in ASCE 41. This work is part of a larger investigation examining the correlation between ASCE 7 and ASCE 41 to identify similarities and differences in the seismic performance of buildings designed using these two standards [8–11]. Project results are intended to provide the technical background for provisions that target equivalent seismic performance in new and existing buildings and to spur further development of PBSO.

Abbreviations

BSE	Basic Safety Earthquake
BPON	Basic Performance Objective Equivalent to New Building Standards
BRBF	Buckling-restrained braced frame
CP	Collapse Prevention
DCR <sub>(N)</sub>	Demand-capacity ratio (normalized)
ELF	Equivalent lateral force
EQ	Earthquake
LDP	Linear dynamic procedure
LS	Life Safety
LSP	Linear static procedure
MCE <sub>R</sub>	Maximum Considered Earthquake (risk-targeted) in ASCE 7
NDP	Nonlinear dynamic procedure
NSP	Nonlinear static procedure
PBSO	Performance-based seismic design
RSA	Response spectrum analysis
SDC	Seismic Design Category
SFRS	Seismic force-resisting system

2. Building design

Six archetype buildings (two at 4-, 8-, and 16-stories) are investigated in this paper. Each building is designed in accordance with the 2012 *International Building Code* (IBC) [12] and its referenced standards (i.e., ASCE 7-10 and AISC 341-10 [13]). Detailed information regarding building properties, materials, and the design process can be found in [14]. The SFRS for each building is a three-bay special moment frame in the east-west direction and a two-bay BRBF in the north-south direction. The braced frame bays in the 4- and 8- story buildings are

symmetrically located and separated by a collector bay, whereas the two bays in the 16-story building are contiguous. Figs. 1 and 2 show the building floor plans and BRBF elevations, respectively. This paper only discusses the performance of the BRBFs, information regarding the moment frame can be found in Harris and Speicher [8].

For determining seismic loads, the buildings are assigned to the upper limit of Seismic Design Category (SDC) D with spectral accelerations at 0.2 s ( $S_S$ ) and 1.0 s ( $S_I$ ) equal to 1.5 g and 0.6 g, respectively (though  $S_I$  is treated to be just less than 0.6 g to avoid additional requirements in ASCE 7). For each building height, two designs are produced: one design using demands determined by the ELF procedure and a second design using demands determined by the RSA procedure. Two designs are produced to provide a common range of potential system strengths for the selected SDC, and to a lesser extent, to compare results obtained from the two design methodologies. The seismic analysis and design parameters for each archetype building are summarized in Table 1.

The frames are designed for wind in accordance with IBC requirements. For determining wind loads, the basic wind speeds are set to 177 km/h (110 mph) for the 700-year (strength) and 116 km/h (72 mph) for the 10-year wind (drift). Though wind is considered, seismic loads control the design of the braces, except for some of the lower stories of the 16-story frame as indicated by the wind-to-seismic story shear comparisons shown in Fig. 3. To compare the story demand to story strength (capacity), an approximate story strength,  $V_{story}$ , is calculated by assuming the frame acts as a truss with pinned connections:

$$V_{story} = \frac{x(\phi_c P_n)L}{\sqrt{h^2 + L^2/4}} \tag{1}$$

where  $x$  is the number of braced bays per story,  $\phi_c P_n$  is the brace compression strength,  $L$  is the bay width, and  $h$  is the story height. Note, Eq. (1) works well when the brace bays are separated, but when the brace bays are contiguous the global flexural action in the frame causes unequal load sharing in the braces at a particular floor, therefore this approximation becomes less accurate.

Regarding the BRBF designs, a chevron bracing configuration is used in the 4-story building and two-story X-bracing is used in the 8- and 16-story buildings. For the 4- and 8-story buildings, the braced bay width is 6.10 m (20 ft.). For the 16-story building, the braced bay width is increased to 9.14 m (30 ft.) and the braced bays are placed adjacent to each other to increase frame stiffness, thus limiting drift and allowing for strength-controlled braces. The braces are designed assuming a

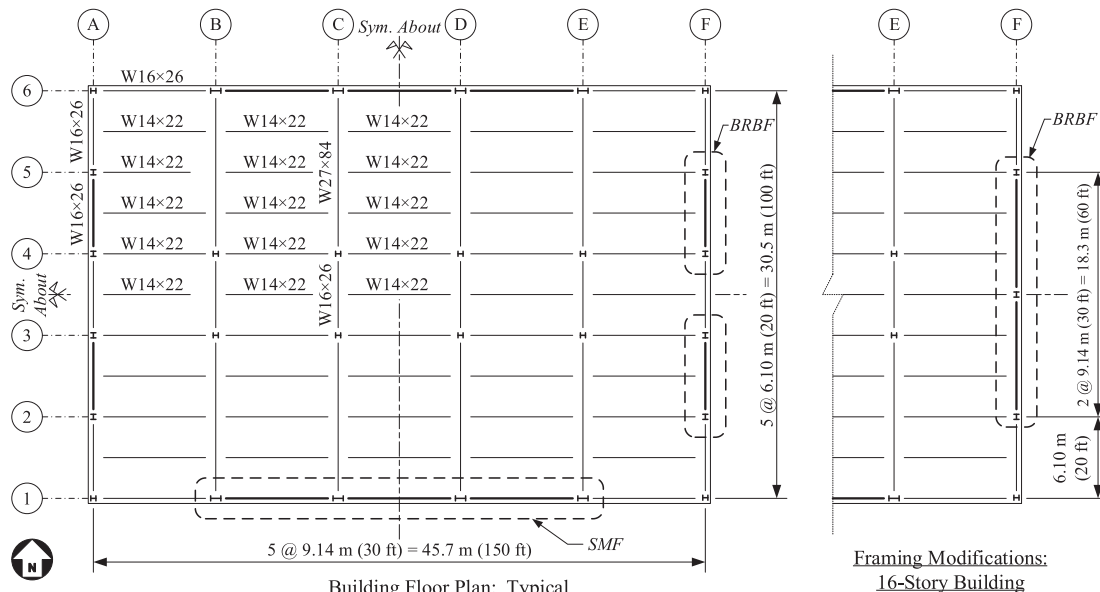


Fig. 1. Typical floor plan for the buildings.

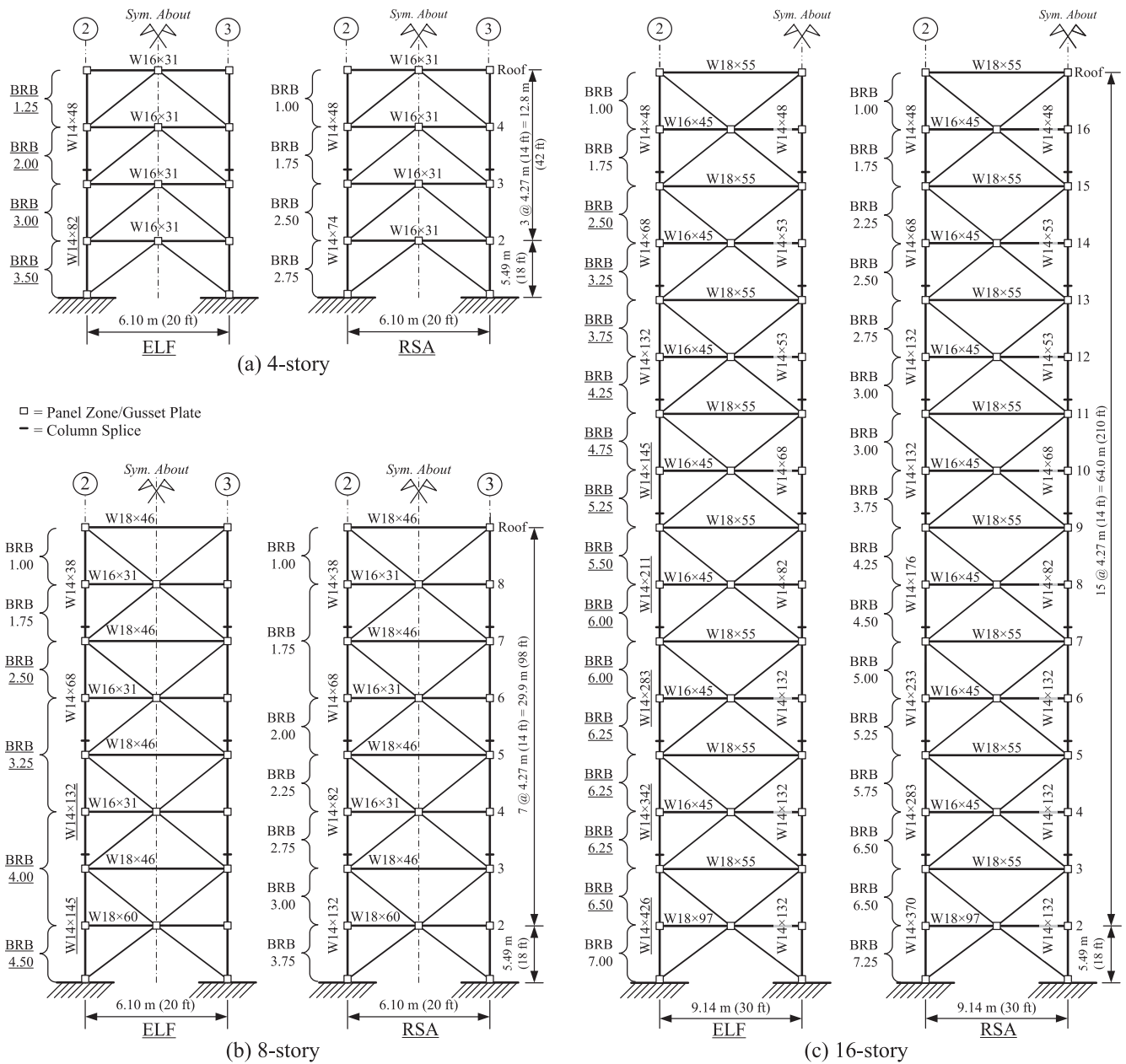


Fig. 2. BRBF elevations for the (a) 4-story, (b) 8-story, and (c) 16-story buildings (note: all structural shapes are given using U.S. designation, BRBF sizes signify core area in units of in<sup>2</sup>, where 1 in<sup>2</sup> = 645 mm<sup>2</sup>).

lower bound brace core strength,  $F_{y,min}$  of 0.269 kN/mm<sup>2</sup> (39 ksi).

The beams are sized to remain elastic under the full unbalanced load as prescribed by AISC 341 [13], though the unbalanced load in a BRBF tends to be small and is upward (thus counter-acting gravity loads). The beam is spliced just beyond of the brace-to-beam connection to create a pinned connection at the edge of the gusset plate (refer to AISC 341 Figure C-F2.8 [13], proposed by Thornton and Muir [15]). This pinned connection is selected because ASCE 41 does not prescribe flexural acceptance criteria for beam-to-column connections when a brace is present. This approach also provides a design that reduces the reliance on the contribution of non-brace assemblies for stiffness and strength.

The design demand-capacity ratios (DCRs) for the braces on the bottom of each two-story pair are kept reasonably uniform over the height of the building as shown in Fig. 3(c). Capacity design requirements in AISC 341 are satisfied for the BRBF beams and columns. The amplified seismic load is taken as the forces developed assuming all braces have forces corresponding to their adjusted strength in

compression or in tension. The BRBF member sizes are shown in Fig. 2 with underlined member sizes in the ELF-designed frames indicating changes from the RSA-designed frame.

### 3. Modeling and analysis setup

For the linear analysis procedures, the buildings are modeled in three dimensions in ETABS [16]. The brace-to-beam and brace-to-column connection is assumed to be made with a gusset plate. The stiffness of the gusset plate connection is approximated by doubling the adjacent member stiffnesses over an estimated plate length of 0.46 m (18 in.). At the end of the gusset plate, the beam is spliced with a shear tab connection which is considered to act as a pinned connection. The floor slabs are modeled as semi-rigid membrane diaphragms with no out-of-plane bending stiffness and a 0.5 in-plane stiffness modifier to account for cracking at design loads. Gravity load-carrying framing is modeled to capture  $P-\Delta$  effects. The gravity beams are modeled with

**Table 1**  
ASCE 7 seismic analysis and design parameters.

Building	4-story		8-story		16-story	
$R, C_d, \Omega_o^a$	8, 5, 2.5		8, 5, 2.5		8, 5, 2.5	
$C_u T_a^b$ (seconds)	0.91		1.48		2.37	
ELF permitted?	Yes		Yes		Yes	
Height limit (m)	73		73		73	
Analysis procedure	ELF	RSA	ELF	RSA	ELF <sup>g</sup>	RSA
$W^c$ (kN)	22,880	22,720	46,750	46,620	97,320	96,510
$V_b^c$ design (kN)	1890	1590	2360	2000	42,840	3610
$V_b^c$ drift (kN)	1450	1820	1930	1910	2810	2340
RSA scaling factor ( $g$ ) <sup>d</sup>	NA	Design = 0.14 Drift = 0.63	NA	Design = 0.17 Drift = 0.63	NA	Design = 0.19 Drift = 0.63
$T_1^e$ (seconds)	1.00	1.11	2.06	2.35	2.60	2.90
Steel weight <sup>f</sup> (kN)	80	71	205	240	1330	1170

Notes:  
<sup>a</sup>  $R$  = response modification factor,  $C_d$  = deflection amplification factor, and  $\Omega_o$  = overstrength factor – see ASCE 7 Table 12.2-1.  
<sup>b</sup> Product of the coefficient for upper limit on calculated period,  $C_u$ , and the approximate period,  $T_a$  – see ASCE 7 Section 12.8.2.  
<sup>c</sup> Inertial mass computed from Dead + Superimposed Dead +  $0.2 \times$  Floor Live.  
<sup>d</sup> Scaling for design =  $g \times I_c/R \times (0.85 \times V_{b,ELF}/V_{b,RSA})$ . Scaling for drift =  $g \times I_c/R \times C_d/I_e$ . The spectrum is defined as a function of  $g$ .  
<sup>e</sup> Fundamental period, computed from a second-order eigenvalue analysis with Dead + Superimposed Dead +  $0.25 \times$  Floor Live gravity load.  
<sup>f</sup> Per single SFRS and does not include connection or miscellaneous steel.  
<sup>g</sup> The 16-story BRBF is technically *not* permitted to be designed with the ELF procedure because its design period,  $C_u T_{a,16}$ , is  $> 3.5 \times T_s$ , where  $T_s$  is  $S_{D1}/S_{D5}$ . Regardless, this design is included for comparison.

pinned connections to minimize their strength and stiffness contributions to the seismic performance.

The BRBs are modeled using single elements connecting working points (w.p.). These elements are assigned an area equal to the specified steel core area. The brace ends are modeled as pinned. Since the actual stiffness of the BRB is higher than  $A_c E/L_{w,p}$ . (where  $A_c$  is the steel core area,  $E$  is the elastic modulus,  $L_{w,p}$  is the length between w.p.), due to the stiffened portion outside the reduced core and the accompanying connection zone (gusset plate, member depths, etc.), a stiffness modifier,  $KF$ , is applied. This is done by first getting an approximate  $KF$  value calculated based on length, core area, and adjacent beam and column members. Next, rather than using a different  $KF$  value for each brace in a building, the average  $KF$  is used to simplify input for both the design and assessment. The difference in building period using the individual  $KF$  values and the average is found to be negligible (less than 2%). For the linear procedures, the braces are assessed assuming an expected yield strength,  $F_{y,es}$ , equal to 1.1 times the lower bound yield strength,  $F_{y,min}$ .

For the nonlinear analysis procedures, the buildings are modeled in

three dimensions using PERFORM-3D [17]. The models are assigned 3% modal damping and 0.3% Rayleigh stiffness proportional damping. The modeling approach is similar to that used for the linear analysis procedures except discrete nonlinear elements are added. The inelastic axial behavior of a brace is modeled using a nonlinear BRB compound component that consists of an inelastic portion and an elastic portion combined in series. The inelastic component (i.e., nonlinear axial hinge) is calibrated using test results from two BRB manufacturers. These tests can be found in reports by Merritt et al. [18] (for Star Seismic) and Newell et al. [19] (for CoreBrace). Specimens 1 [18] and 1G [19] are used for the calibration and have core areas of 2260 mm<sup>2</sup> (3.5 in<sup>2</sup>) and 7740 mm<sup>2</sup> (12 in<sup>2</sup>), respectively, and yield zone length,  $L_{yz}$ , of 4.47 m (176 in.) and 3.44 m (136 in.), respectively. Both reports note that the deformation portion of the force-deformation data includes a small amount of elastic deformation from the area outside the yielding zone of each brace due to placement of string potentiometers. For Specimen 1, the string potentiometers were mounted on the clevis attached directly to the supports. This resulted in a small portion of near-zero stiffness due to a gap (from both practical tolerance limits and

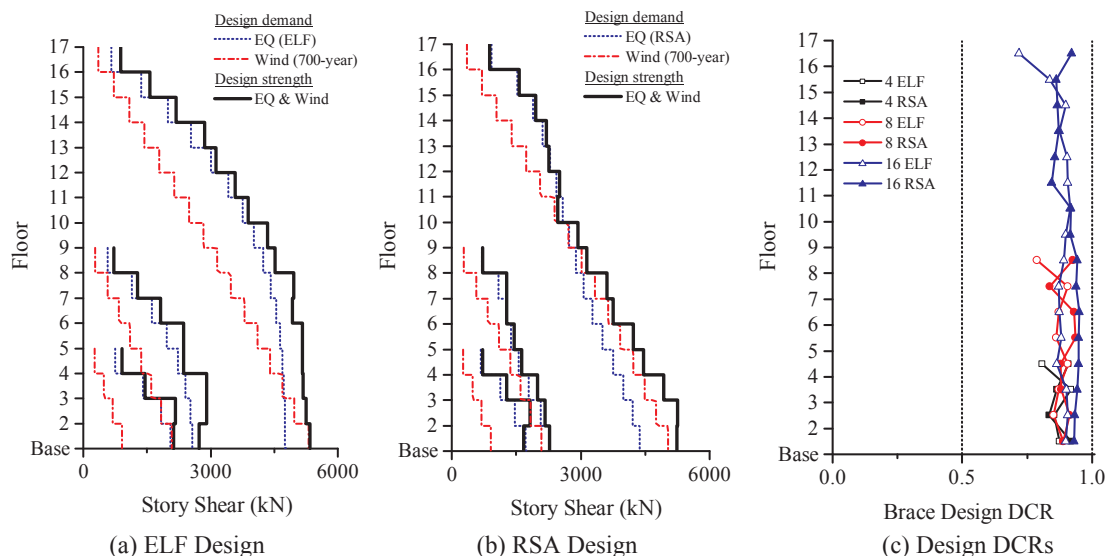


**Fig. 3.** Select design information in terms of (a) story shear demands and nominal strengths for the ELF-designed BRBFs, (b) story shear demands and nominal strengths for the RSA-designed BRBFs, (c) and design DCRs for braces for all BRBFs.

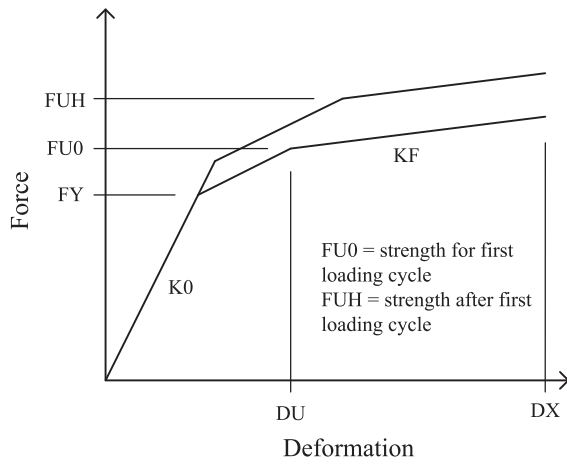


Fig. 4. Force-deformation plot showing the PERFORM-3D BRB inelastic component model property definitions (see [17] for more on input variable definitions).

pin-hole elongation) between the pin and the clevis. This gap-effect is minor and thus is neglected in the calibration and modeling.

Fig. 4 shows the parameters needed to define the force-deformation behavior in the PERFORM-3D inelastic component. Table 2 gives the corresponding values used in the brace models.  $FY$  and  $FU0$  are nearly the same in tension and compression, therefore the same value is used for both. The length of the inelastic component is set equal to the length of the yield zone,  $L_{yz}$ . The length of the elastic bar component,  $L_{bar}$ , is set equal to  $L_{w.p.} - L_{yz}$ . To determine the area of the elastic bar component, a target stiffness,  $K_{target}$ , is set as follows:

$$K_{target} = KF \frac{A_c E}{L_{w.p.}} \quad (2)$$

where  $KF$  is the average stiffness modifier determined in design (usually provided by the brace manufacturer). Given this target stiffness, the needed elastic stiffness of the bar,  $K_{bar}$ , and bar area,  $A_{bar}$ , are:

$$K_{bar} = \frac{K_{target} K_{yz}}{(K_{target} + K_{yz})} \quad (3)$$

$$A_{bar} = K_{bar} \frac{L_{bar}}{E} \quad (4)$$

PERFORM-3D's endzone option is not used for the BRB because the endzones are implicitly accounted for in  $KF$ .

To demonstrate the model fit, Fig. 5 shows the force-deformation results of the model compared to experimental data using  $A_c = 2900 \text{ mm}^2$  (4.5 in.<sup>2</sup>) and  $L_{yz} = 3.30 \text{ m}$  (130 in.). The hardening behavior selected is "maximum deformation only", 2.0 for maximum deformations at  $FU - FUH$ , and 3.5 for maximum deformations at  $FUH$  (see PERFORM-3D user manual [20]). The stiffness, strength, and strain hardening behavior of the BRB model match well with the experimental results. Using tests from different manufactures assists in making the analysis model applicable to a generic BRB component independent of manufacturer. The experimental results are limited to brace core strains of approximately 0.017 for Specimen 1G and approximately 0.023 for

Table 2  
Inelastic component properties used in BRB model calibration.

Variable	$K0$	$KF$	$FY$	$FU0$	$FUH (T^c)$	$FUH (C^f)$	$DU$	$DX$
Value	$K_c^a$	$0.02K_{target}^b$	$0.89P_{y,c}^c$	$1.05P_{y,c}$	$1.34P_{y,c}$	$1.51P_{y,c}$	$0.0058L_{yz}^d$	$0.04L_{yz}$

<sup>a</sup>  $K_c$  = steel core stiffness.  
<sup>b</sup>  $K_{target}$  = targeted brace overall elastic stiffness.  
<sup>c</sup>  $P_{y,c}$  = steel core yield force.  
<sup>d</sup>  $L_{yz}$  = length of yielding zone,  $0.0058L_{yz} = 0.7$  when  $L_{yz} = 3.0 \text{ m}$  (120 in.), and for other  $L_{yz}$  values the number changes proportionally.  
<sup>e</sup> T = tension.  
<sup>f</sup> C = compression.

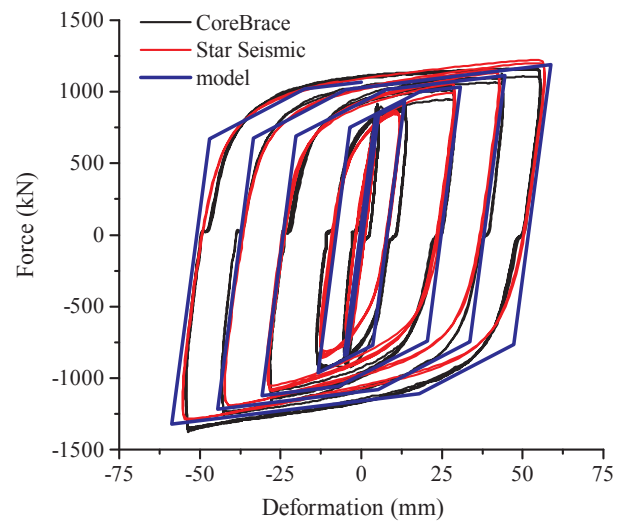


Fig. 5. Comparison of BRB inelastic model to experimental results from data reported in Merritt et al. [18] (Star Seismic) and Newell et al. [19] (CoreBrace).

Specimen 1 (data was truncated at 0.017 for the calibration). Given that the story height and bay width of the archetype frames are 4.27 m (168 in.) and 6.10 m (240 in.), respectively, every 1.0 mm stretch of the brace corresponds to 1.72 mm of drift ( $= L_{w.p.}/b/2 = 5.25/(6.10/2)$ ). Therefore, for reference when examining the results, a yield zone strain of 0.017 for a BRB with a 3.30 m (130 in.) yield zone length equates to a drift level of approximately 0.023 radians ( $= 0.017 \times 3.30 \times 1.72/4.27$ ), or 2.3%, ignoring the elastic strain in the region outside the yield zone.

Though the BRB yield zone is only calibrated using deformations up to  $0.017 L_{yz}$ , the deformation capacity of the BRB,  $DX$  in Fig. 4, is set to  $0.04 L_{yz}$  with the force-deformation further extrapolated with no strength loss capabilities. The expected yield stress,  $F_{ye}$ , is assumed to be established from testing and is taken as  $0.317 \text{ kN/mm}^2$  (46 ksi). The expected axial yield deformation of the brace,  $\Delta_y$ , is  $L_{yz} \times F_{ye}/E = L_{yz} \times 0.317/200 = 0.00159 L_{yz}$ . Per ASCE 41 Table 9-6, generalized deformation parameters  $a$  and  $b$  both equal 13.3  $\Delta_y = 13.3 \times 0.00159 L_{yz} = 0.021 L_{yz}$ , which also corresponds to the Collapse Prevention (CP) acceptance criteria. Therefore, the strain in the brace core at the CP permissible deformation is  $\Delta_y + 13.3 \Delta_y = 14.3 \Delta_y = 14.3 \times 0.00159 L_{yz} = 0.023 L_{yz}$ , which corresponds to the maximum deformations reported in Specimen 1. Values beyond this deformation should be treated with caution although it is anticipated that, for tension, the core strains could reach upwards of 20–30% before fracture occurs. For compression, the yielding core stiffness would begin to increase at large strains as the confining action of the mortar and hollow structural section shell restrain the Poisson effect. It is not clear whether this phenomenon would overcome the tensile fracture of the adjacent brace and repel further ductility demands by shifting demands to adjacent floors. Regardless, fracture and strain hardening due to confinement is not captured in the model used in this study. It is assumed once deformation values exceed the CP permissible

deformation limit, a non-simulated failure has occurred and collapse may be imminent. Values obtained after a component reaches the CP limit should be treated with caution due to the realization that the response is beyond the range of model calibration and beyond commonly accepted drift limits.

Though significant nonlinearity is not anticipated in members other than in the braces due to capacity design requirements in AISC 341, moment-curvature hinges are placed in the beams and columns adjacent to the brace connections to capture potential nonlinear flexural response. Additionally, panel zones are modeled with a nonlinear panel zone component model provided in PERFORM-3D.

The nonlinear analysis is set to terminate when the solution fails to converge or when an arbitrary roof drift ratio of 20% is reached. Although convergence limits and drift limits are often used as an indicator of collapse, in this study collapse is evaluated by using the assessment criteria alone (via component limits in ASCE 41 Table 9-6 and Table 9-7). Collapse modes not modeled herein (e.g., failures in the gravity framing system) would likely occur well before 20% is reached, plus nonlinear components would be beyond their valid range of modeling. Other than above, roof drift is not used nor discussed in regard to the performance of a structure assessed with ASCE 41. Additional information on modeling details and the selection of PERFORM-3D analysis parameters can be found in [14].

## 4. Seismic performance assessment

### 4.1. Performance objective

The target seismic performance objective selected for this study is the Basic Performance Objective Equivalent to New Building Standards (BPON) as defined in ASCE 41 Table 2-2. This objective has the dual goal of Life Safety (LS) at the Basic Safety Earthquake-1N (BSE-1N) and Collapse Prevention (CP) at the BSE-2N. In this objective, BSE-2N is taken as the risk-targeted Maximum Considered Earthquake,  $MCE_R$ , as defined in ASCE 7 and the BSE-1N is taken as  $2/3 \times BSE-2N$ . This selection allows a comparison between the seismic performance objective intended by ASCE 41 and the seismic design objective intended by ASCE 7 for an “ordinary” building. The only explicit connection between the target structural performance objectives of the BPON in ASCE 41 and the design performance objective in ASCE 7 is “collapse prevention” given maximum considered earthquake shaking, assuming the BSE-2N is equivalent to the  $MCE_R$  defined by ASCE 7.

The definition of CP is subjective and the way to achieve this concept varies between the two standards. In ASCE 7, CP is provided when there is a 90% confidence that a partial or total collapse will not occur given an  $MCE_R$  event; it is presumed that an appropriately designed structure using a seismic hazard of  $2/3 \times MCE_R$  will achieve this design performance objective. In ASCE 41, CP is provided when all component demands do not exceed a limiting threshold for an  $MCE_R$  event. However, equating the two performance objectives is challenging based on a binary member-level performance solution in which a member passes or fails the component limits. Consequently, the question becomes: what percentage of components needs to fail the associated CP performance level in ASCE 41 to achieve the 10% conditional probability in ASCE 7? The assessment results presented herein focus only on CP at the BSE-2N as it tends to be the more critical case. Assessment results for LS at the BSE-1N can be found in [14].

### 4.2. Acceptance criteria

Compliance with a performance objective in ASCE 41 is checked by verifying that component demands do not exceed acceptance criteria dependent on the performance level, component type, and designation (i.e., *primary* or *secondary*). Acceptance criteria for components in linear assessment procedures are provided as  $m$ -factors. Acceptance criteria for components in nonlinear assessment procedures are provided as

plastic deformations. Component actions (e.g., bending) are classified as either deformation-controlled (ductile behavior) or force-controlled (non-ductile behavior). BRBF components are designated as *primary* load carrying members and axial component actions in the braces are considered deformation-controlled. Component actions in the columns and beams are either force or deformation-controlled depending on the axial load demands (see ASCE 41 §9.5.4.4.1). Brace connections are force-controlled, but are not assessed in this paper.

In this study the results for both the linear and nonlinear assessment procedures are presented in terms of a *normalized* demand-capacity ratio,  $DCR_N$  (the  $N$  subscript is added to distinguish it from the  $DCR$  defined in ASCE 41 §7.3.1.1). As such, a  $DCR_N$  value greater than unity indicates that a component does not satisfy the acceptance criteria (and is denoted by red-bolded and underlined text in the results presentation).

For the linear analysis results,  $DCR_N$  is defined in Eqs. ((5) and (6)):

$$\text{Deformation-controlled: } DCR_N = \frac{Q_{UD}}{m\kappa Q_{CE}} = \frac{DCR}{m\kappa} \quad (5)$$

$$\text{Force-controlled: } DCR_N = \frac{Q_{UF}}{\kappa Q_{CL}} \quad (6)$$

where  $Q_{UD}$  is the deformation-controlled demand,  $Q_{UF}$  is the force-controlled demand,  $Q_{CE}$  is the expected strength,  $Q_{CL}$  is the lower-bound strength,  $m$  is the component demand modification factor, and  $\kappa$  is the knowledge factor (taken as unity in this study).

For the nonlinear analysis results,  $DCR_N$  is defined in Eqs. ((7) and (8)):

$$\text{Deformation-controlled: } DCR_N = \frac{Q_{UD}}{\kappa Q_{CE}} = \begin{cases} \text{Total} & \frac{\theta_{plastic} + \theta_{elastic}}{\kappa(\theta_y + \theta_{pe} + \theta_{p,AC})} \\ \text{Plastic} & \frac{\theta_{plastic}}{\kappa\theta_{p,AC}} \end{cases} \quad (7)$$

$$\text{Force-controlled: } DCR_N = \frac{Q_{UF}}{\kappa Q_{CL}} \text{ and } DCR_N = \frac{\theta_{total}}{\kappa\theta_y} \quad (8)$$

where  $\theta_{plastic}$  is the plastic deformation,  $\theta_{elastic}$  is the elastic deformation,  $\theta_y$  is the expected yield deformation,  $\theta_{pe}$  is the post-yield elastic deformation,  $\theta_{total}$  is the total deformation, and  $\theta_{p,AC}$  is the acceptance criterion based on plastic deformation. For steel components in ASCE 41, inelastic deformation parameters are provided in terms of plastic deformations rather than total deformations. The choice of whether to use plastic deformations or total deformations will depend on what nonlinear component model is adopted for each component action (e.g., moment-curvature hinge or moment-rotation hinge). Consequently, yield and post-yield elastic deformations may need to be added to the values given in ASCE 41 to determine the total deformation for each structural performance metric. For the axial deformation in the BRBs, results from PERFORM-3D are given in terms of total deformations and these total deformations are used directly in the assessment.

### 4.3. Seismic hazard

The seismic hazard is defined in ASCE 41 §2.4. For the BSE-2N,  $S_S = 1.5$  g and  $S_1 = 0.6$  g. Assuming stiff soil within Site Class D, the resulting design spectral accelerations at 0.2 s ( $S_{XS}$ ) and 1.0 s ( $S_{X1}$ ) are 1.5 g and 0.9 g, respectively.

For the nonlinear dynamic analysis, 14 ground motions are selected from a set of 44 records (22 pairs) used in FEMA P695 [21]. The records are selected by picking the scaled spectra for an individual motion that most closely matches the  $MCE_R$  spectrum between 0.2  $T_1$  and 1.5  $T_1$ . The 14 (best-fit) selected records are then scaled so that the average spectrum does not fall below the  $MCE_R$  spectrum within the same period range. The scaled record set for each building is then taken directly as the BSE-2N. Complete details of the earthquake records used for each building (six sets) and the scaling process can be found in

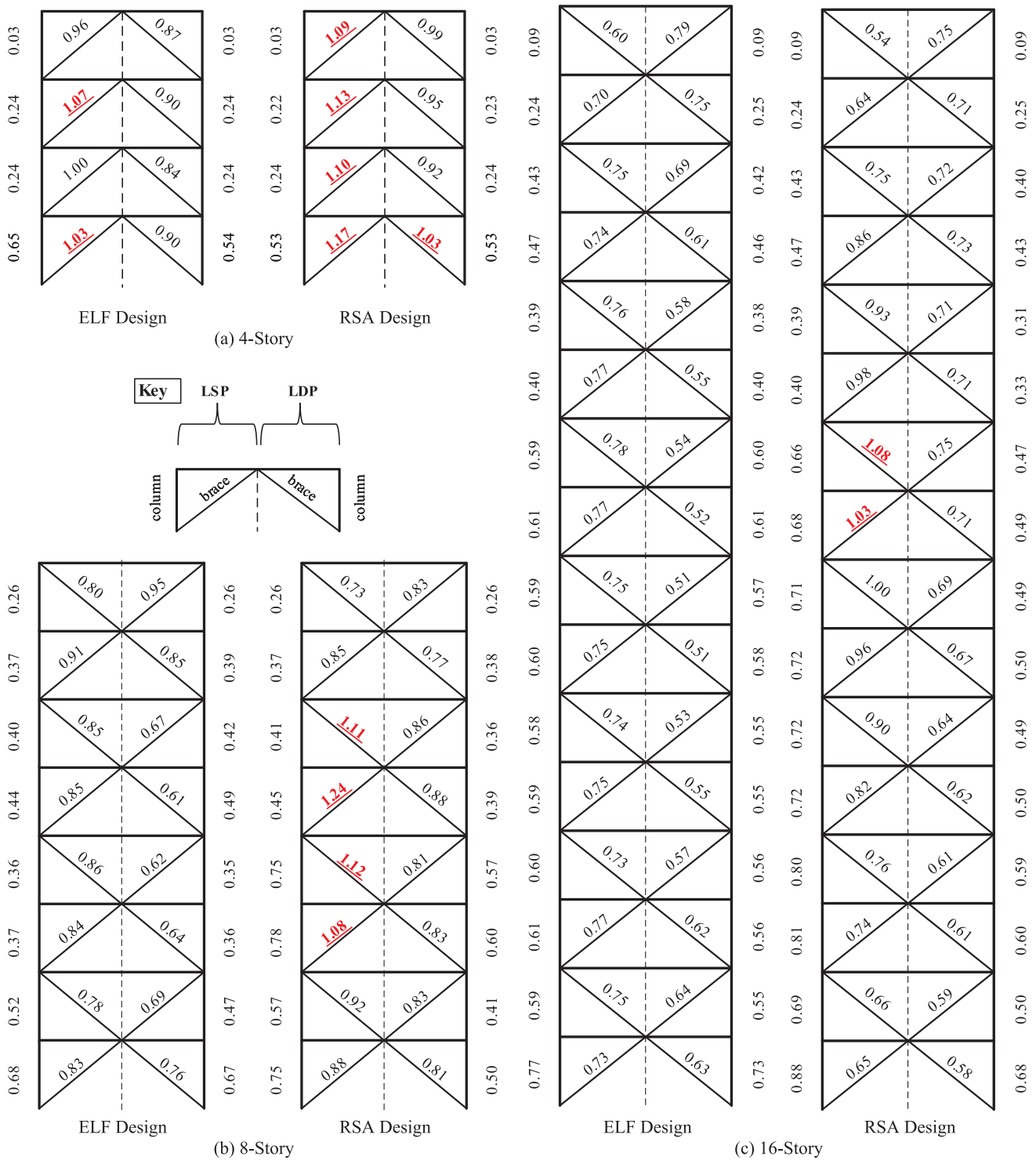


Fig. 6. LSP and LDP assessment results in terms of  $DCR_N$  for CP at the BSE-2N.

Speicher and Harris [14]. The selected earthquakes for each building are referred to herein as EQ 1 - EQ 14 for brevity.

#### 4.4. Linear assessment results

The assessment results from the linear static procedure (LSP) and linear dynamic procedure (LDP) for CP at the BSE-2N are shown in Fig. 6. The deformation-controlled braces do not satisfy the assessment criteria for all designs. The  $DCR_N$  values for the braces range from

approximately 0.5 to 1.2, with the ratios remaining fairly uniform with overall building height and as one moves up the elevation of the building. The majority of the failures occur in the RSA-designed frame assessed using the LSP. This result indicates the sensitivity of assessment results to variations between design and assessment lateral force distributions (i.e., using LSP to assess the RSA-designed frame). The columns satisfy the assessment criteria in all the frames. The beams are not explicitly assessed here because they are capacity protected in design.

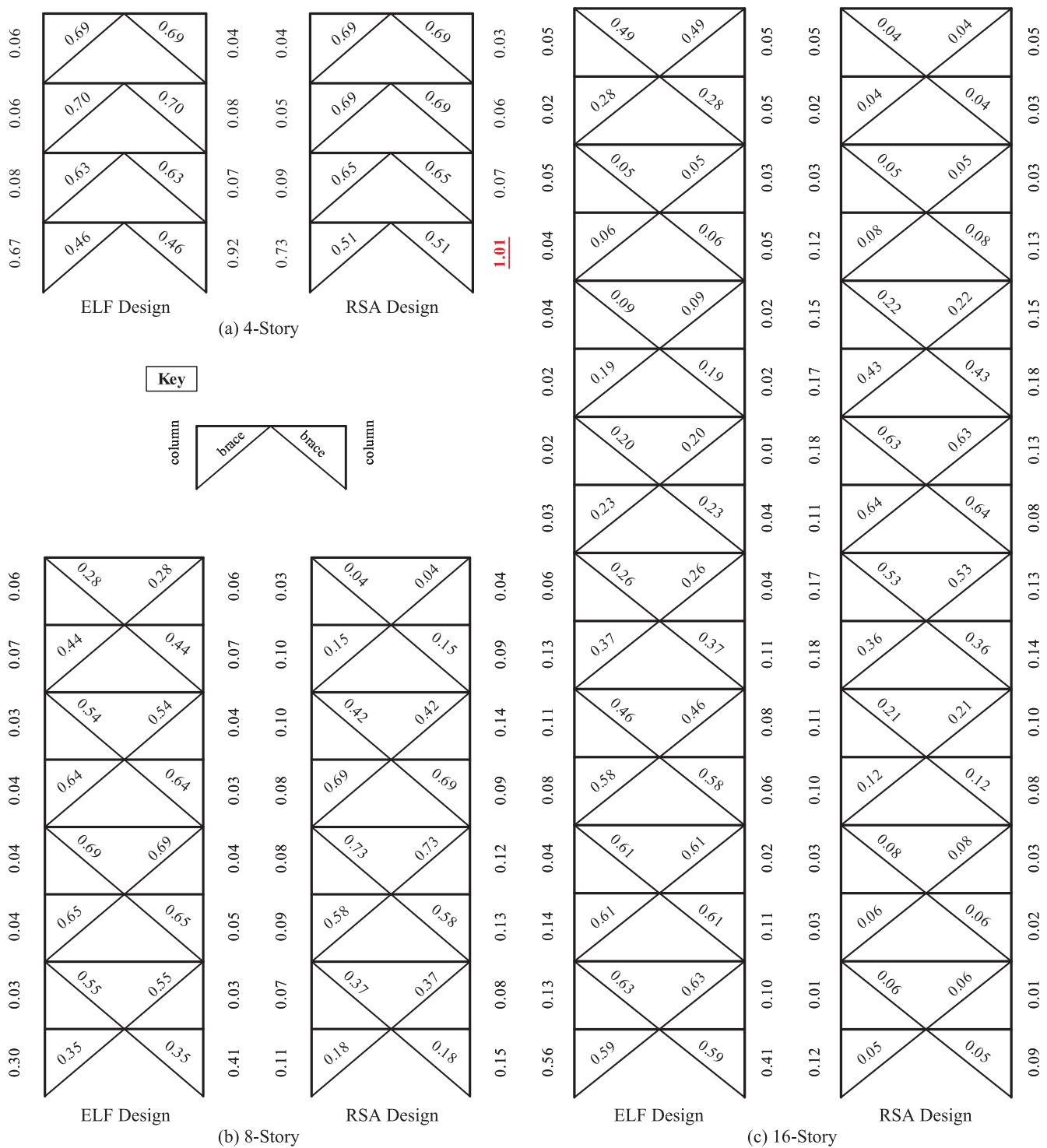


Fig. 7. NSP assessment results in terms of  $DCR_N$  using CP (braces) and yield (columns) for the BSE-2N.

#### 4.5. Nonlinear assessment results

##### 4.5.1. Nonlinear static procedure (NSP)

The assessment results from the NSP for CP at the BSE-2N are shown in Fig. 7. In this analysis, the column results utilize yield deformation as the acceptance criterion in the  $DCR_N$  calculation (see Eq. (8)), therefore the results are implicitly assuming the columns are force-controlled for flexure. Note, the columns are only force-controlled for flexure when  $P/P_{CL} > 0.5$  (where  $P$  is the axial compression load and  $P_{CL}$  is the lower-bound compression strength), which tends to be columns in the lower

portion of the frame (see [14] for further details).

The results reported in the figure are taken from the maximum of each respective member type, ignoring direction of loading or load effect (compression or tension). While this envelope approach illustrates performance failures, it may not provide a clear picture of the mechanism or retrofit strategy.

The results indicate the BRBFs successfully pass the assessment criteria except for the base column in the 4-story RSA-designed frame, but by only a small margin. After further inspection of the initial force-controlled assumption, this column should be treated as deformation-

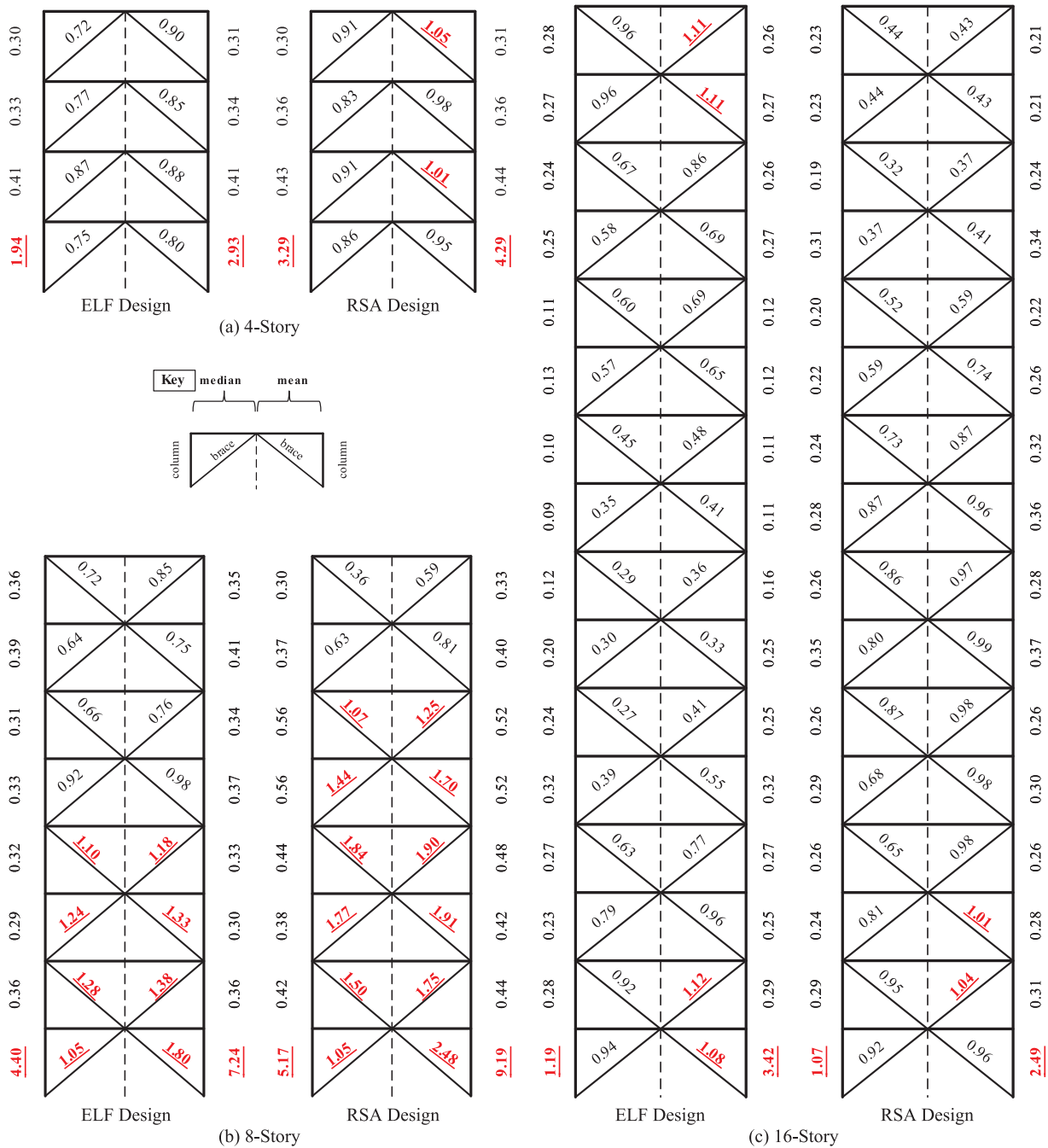


Fig. 8. NDP assessment results in terms of  $DCR_N$  for CP (braces) and yield (columns) at the BSE-2N.

controlled because the  $P/P_{CL} < 0.5$ . Therefore, this column will pass the acceptance criteria.

4.5.2. Nonlinear dynamic procedure (NDP)

The assessment results from the NDP for CP at the BSE-2N are shown in Fig. 8.  $DCR_N$  values are given for median and mean responses for the record set to compare the difference between these two statistics. The results for the beams satisfy the acceptance criteria and are not reported in the figure. The statistics are calculated at the member level using the maximum of the tension  $DCR_N$  and compression  $DCR_N$  for each ground motion (i.e., the distinction between tension and compression is lost after the  $DCR_N$  is first calculated). To simplify the presentation, the results are further condensed by taking the maximum mean and maximum median for the two braces at each level and then reporting these values in the left and right braces, respectively, in Fig. 8.

For the 4-story frames, all braces pass the assessment criteria using median and mean values except for the mean values of the 2nd and 4th floor braces in the RSA-designed frame. The base columns also yield in both 4-story frames, and since these columns are classified as force-controlled for flexure, they fail the assessment. For the 8-story buildings, both the ELF- and RSA-designed frames have many braces that fail the assessment criteria when using both the median and mean values. Specifically, the failures occur from the bottom to the mid-height of both frames. The 2nd and 3rd floor braces in the ELF-designed frame and the 3rd and 4th floor braces in the RSA-designed frame have the highest median  $DCR_N$  values. Moderate concentrations of deformation demand can be seen in the lower stories, but overall the demands are reasonably distributed over the height of the frame. The force-controlled columns also yield as seen in the 4-story frames. For the 16-story buildings, brace performance for both the ELF- and RSA-designed

**Table 3**  
Performance summary of brace members per frame for the linear procedures.

Archetype	Design	LSP	LDP
4-Story	ELF	(4) Fail 50%	Pass
	RSA	(8) Fail 100%	(2) Fail 25%
8-Story	ELF	Pass	Pass
	RSA	(8) Fail 50%	Pass
16-Story	ELF	Pass	Pass
	RSA	Pass	Pass

frames is better than that seen in the 8-story frames, with all median brace results satisfying the assessment criteria. With respect to the mean results, several of the 16-story braces fail the assessment, but only by approximately 10% or less. The columns similarly fail the assessment criteria, though the median only fails by approximately 20% or less.

Comparing the two statistics reported, the mean values are consistently higher than the median values, as is expected. The difference in the results of the ELF- and RSA-designed frames is minimal, with the ELF-designed frame performing slightly better in most cases. Technically no design passes the assessment criteria, though the 4-story ELF-designed frame only has issues with the first story column.

**5. Discussion of assessment results**

In general, the ASCE 41 performance assessment indicates mixed performance results for the BRBF; the 4-story and 16-story frames generally perform well, while the 8-story frame does not. The trends in conservatism among the four different assessment approaches was unexpected. This section discusses these results and makes recommendations for future research and/or targeted changes to assessment provisions. It should be noted that none of the analysis procedures considered herein are adequate for establishing the probability of collapse. If an estimate on the probability of collapse is needed (e.g., to prove ASCE 7 design intent is satisfied), a FEMA P695 assessment should be conducted.

**5.1. Linear assessment**

Table 3 summarizes the performance of the braces for each linear assessment procedure at the CP structural performance level. For the ELF-designed frames, nearly all braces pass the acceptance criteria. The only failures are in the 4-story frame assessed using the LSP, where the 1st and 3rd story braces have  $DCR_N$  values of 1.03 and 1.07, respectively. In contrast, there are several more failures in the RSA-designed frames. The most failures are seen in the 4- and 8-story frames using the LSP. This is not too surprising given the difference between the lateral force distributions of the RSA design (based on a summation of modal responses) and the LSP assessment (based on a single mode shape weight distribution multiplied by story height relative to the base). The  $DCR_N$  values of the braces that fail range from just above unity to 1.24, indicating even the “poorly” performing frames are not failing by a large margin. Regardless, as a comparison, a companion study that looked at the performance of special concentrically braced frames and eccentrically braced frames did not show any failures in the braces or

**Table 4**  
Effect of design and assessment provisions on  $DCR_N$  of a BRB for LS at BSE-1N.

	Demand		Capacity	Effect on $DCR_N$
(a) ASCE 41	$S_a$ at $T = T_{analysis}$	$1/m = 1/5.6$	$P_{CE} = 1.1(F_y A_c)$	$DCR_N = \frac{(\# \le 1.0)(1.43)}{1.22}$ ; $DCR_N \le 1.17$
(b) ASCE 7 and AISC 341	$S_a$ at $T = \min(T_{analysis}, C_u T_a)$	$1/R = 1/8$	$\phi P_n = 0.9(F_y A_c)$	
Ratio (a / b)	$a/b \le 1.0$	$a/b \le 1.43$	$a/b = 1.1/0.9 = 1.22$	

**Table 5**  
Fundamental period comparison for the building suite.

Design procedure	4 -Story		8-Story		16-Story	
	RSA	ELF	RSA	ELF	RSA	ELF
$T_{analysis}$ (s)	1.11	1.00	2.35	2.06	2.90	2.60
$C_u T_a$ (s)	0.91		1.49		2.46	
$C_u T_a / T_{analysis}$	0.82	0.91	0.63	0.72	0.85	0.95

links using the linear assessment procedures [6,7].

To get a better understanding of the relationship between the linear design (ASCE 7 and AISC 341 procedures) and the linear assessment (ASCE 41 procedures), Table 4 summarizes the effects of design and assessment provisions on the  $DCR_N$  for a brace member at  $\frac{2}{3} \times MCE_R$  for the LS structural performance level (this performance and hazard level is used in lieu of CP at BSE-2N to align with that used in design). This table only applies in comparing the ELF to the LSP, since the vertical distribution of lateral forces must be the same for these observations to be valid. On the component capacity side, the axial compression strength of a BRB prescribed in ASCE 41,  $P_{CE}$ , and AISC 341,  $P_n$ , have the same underlying equation; differences arise when using nominal versus expected material properties and a strength reduction factor,  $\phi_c = 0.9$ , resulting in a capacity ratio (ASCE 41/AISC 341) of 1.22. On the component demand side, assuming an eigenvalue analysis is conducted, ASCE 41 allows the use of the period determined from analysis,  $T_{analysis}$ , whereas ASCE 7 will limit this period to the product of the upper limit coefficient and the approximate period,  $C_u T_a$ . If this limit is triggered, the demand in the braces will generally increase for a design resulting in a demand ratio (ASCE 41/ASCE 7) less than unity. Additionally, ASCE 41 effectively divides the demand by  $m$  ( $= 5.6$  for BRB) while ASCE 7 divides the elastic demand by  $R$  ( $= 8$  for an BRBF). Thus, for a BRB designed per ASCE 7 (and its referenced standards) whose nominal strength exactly equals the demand from ASCE 7, the corresponding  $DCR_N$  for the linear assessment will be less than or equal to 1.17, as indicated in Table 4. This value increases to 1.31 for the CP structural performance level at the BSE-2N.

In this study, one of the major factors affecting the final linear procedure results (i.e.,  $DCR_N$  values) is the difference between the fundamental period used in ASCE 7 and ASCE 41. To illustrate this effect, the results of the 8-story ELF-designed BRBF assessed using CP at the BSE-2N is examined. For the design,  $C_u T_a$  (the limit) is 1.49 s (as shown in Table 5). In contrast, the assessment period (calculated using eigenvalue analysis) is 2.06 s. Assuming the period is on the descending branch of the response spectrum, it is evident that the spectral acceleration,  $S_w$ , calculated using the assessment period (2.06 s) will be smaller than that calculated using the design period (1.49 s). Also, the shape of the lateral force distribution is dependent upon the period via the exponent  $k$  in equation 12.8-12 of ASCE 7. This makes the effect of the period difference more complicated than a simple fraction (i.e., the difference is not simply 1.49/2.06). To illustrate this relationship, Fig. 9 shows the variation of  $DCR_N$  (ASCE 41)/ $DCR$  (ASCE 7) for a range of different period combinations. When the periods are equal, the maximum  $DCR_N$  is 1.31 for all stories, as pointed out in the previous paragraph. For the 8-story ELF-designed frame, the respective curve indicates that, for braces designed with  $DCR$  equal to unity, the  $DCR_N$  obtained in the assessment would be between 0.94 and 1.04.

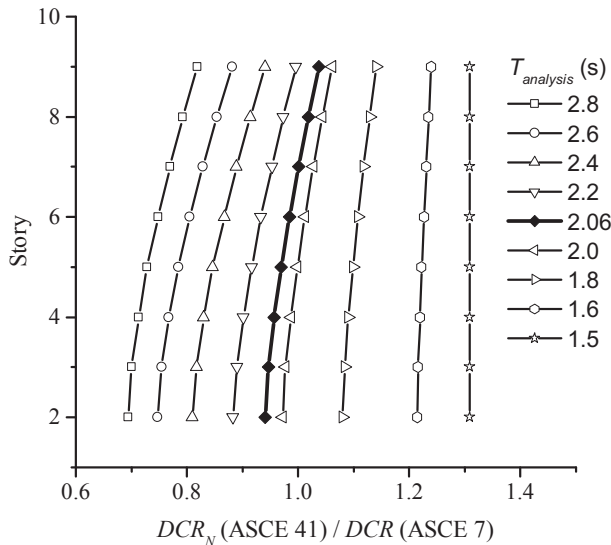


Fig. 9. Example variation of the ratio of brace assessment  $DCR_N$  (i.e., ASCE 41) to the design  $DCR$  (i.e., ASCE 7) based on the 8-story ELF-designed frame assessed using CP at BSE-2N hazard level.

Additionally, Table 6 summarizes the sources of added strength that are inherent in the BRBF design. These include the following: (1) the ASCE 7 design includes both 5% eccentricity and multidirectional seismic effects (e.g., 100% of the earthquake loading in one direction and 30% in the perpendicular direction), neither of which are required nor included in the assessment in this study; (2) certain braces can require additional strength (above that required for seismic) when wind is the controlling lateral load; and (3) practical size limitations, both in increment size and minimum size, can play a role in member selection. The cumulative effects of these requirements resulted in additional strength in the BRBF components, which can further reduce the  $DCR_N$  values obtained from the ASCE 41 assessments.

5.2. Nonlinear assessment

In contrast to a majority of the braces satisfying the linear assessment criteria, a larger number of braces fail the nonlinear assessment criteria. This result is contrary to that expected since the concept of conducting an analysis of increased rigor is to reduce conservatism, potentially resulting in more realistic results.

5.2.1. Nonlinear static procedure

The assessment results from the NSP indicate that the frames consistently pass the CP performance level at the BSE-2N. For reference, the second-order nonlinear static pushover curves are plotted for each building in Fig. 10. Changes in stiffness generally correspond with brace

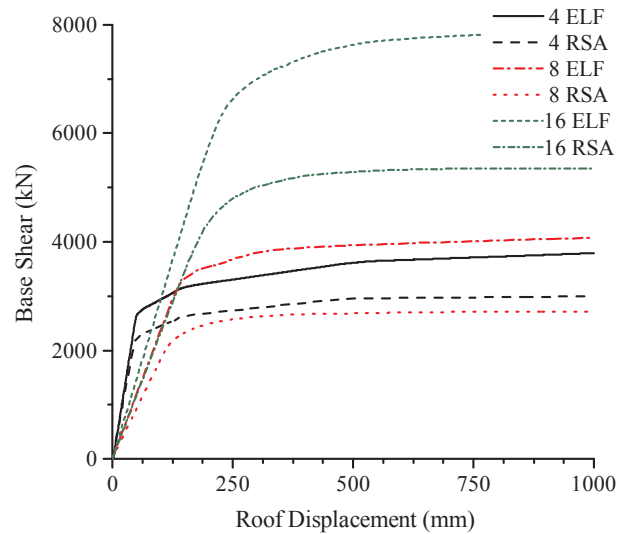


Fig. 10. Second-order nonlinear static pushover curve for the suite of buildings.

core yielding. Once a brace yields, drift begins to accumulate at that story more rapidly than in other stories. This response is illustrated in Fig. 11 for the 8-story ELF-designed frame (note that the 8-story frames have the worst performance of the suite). The 1st story brace yields at 0.36% roof drift, followed by the 3rd, 7th, 5th, and 4th story braces yielding at 0.38%, 0.38%, 0.39%, and 0.42% roof drift, respectively. Drift tends to concentrate more in the 3rd, 4th, and 5th stories at both the BSE-1N and BSE-2N levels. The stable post-yield behavior of the BRBs seems to promote gradual transitions in drift distribution for the frame. Ultimately, the 2nd through 4th floors have the highest  $DCR_N$  values for the 8-story ELF-designed frame, but the members at these floors still pass the CP acceptance criteria (max  $DCR_N$  value of 0.74).

Though the NSP has its deficiencies in capturing how an actual earthquake may deform a building (e.g., does not directly capture effects of changes in stiffness and higher modes), the understanding of the order of brace yielding as the frame is subjected to an increasing “first-mode shaped” lateral load can be beneficial in understanding the deformation demand pattern as part of the assessment process. As is confirmed in this section, the NSP indicates that the middle story braces are the first to see large demands. However, it is generally beneficial to take the next step of selecting ground motions and using the more robust NDP if one goes through the effort of creating a nonlinear model.

5.2.2. Nonlinear dynamic procedure

The assessment results from the NDP are noticeably different than those seen from the NSP. Fig. 8 (presented previously) shows the distribution of failures over the height of the building. Table 7 provides a summary of the performance of the brace members for each nonlinear assessment procedure. All braces pass the NSP. In contrast, there are

Table 6  
Summary of factors contributing to design  $DCR$  (ASCE 7) vs. assessment  $DCR_N$  (ASCE 41) differences.

	ASCE 7	ASCE 41
Period	$T_{used} = \min(C_u T_u, T_{analysis})$ $C_{vx}$ is a function of $k$ , which in turn is a function of $T$ , therefore the force distribution is slightly different between the two standards	$T_{used} = T_{analysis}$
Eccentricity	5% accidental	if $\eta \leq 1.1$ then none required
$C_s$ , seismic response coeff.	$C_s$ shall not be less than $0.044 S_{DS} I_e \geq 0.01$	No limits
Concurrent multidirectional loading	$1.0E_x \pm 0.3E_y$	§7.2.5 permits only the consideration of non-concurrent seismic motions unless there are (1) plan irregularities or (2) intersecting lateral systems
P-Δ effects	Considered	Considered

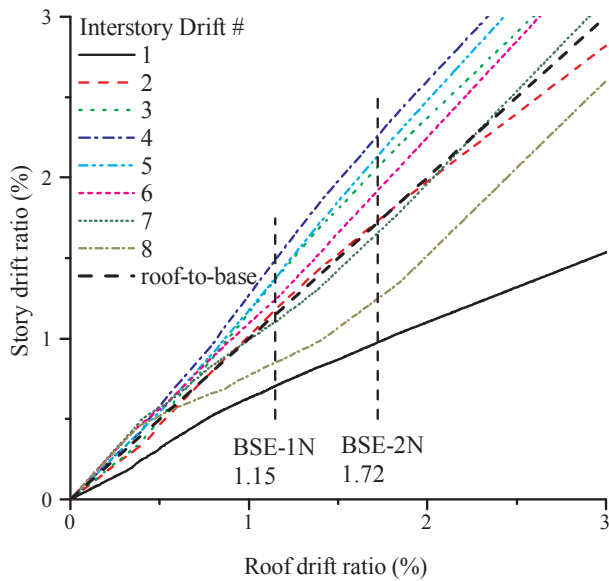


Fig. 11. Drift contributions from each story for the 8-story ELF-designed frame.

**Table 7**  
Performance summary of brace members and column hinges per frame for the nonlinear procedures.

Archetype	Design	NSP		NDP (based on mean response of record set)	
		Brace	Column Hinge	Brace	Column Hinge
4-Story	ELF	Pass	Pass	Pass	(2) Fail 13%
	RSA	Pass	(1) Fail 12%	(2) Fail 25%	(2) Fail 13%
8-Story	ELF	Pass	Pass	(8) Fail 50%	(2) Fail 6%
	RSA	Pass	Pass	(12) Fail 75%	(2) Fail 6%
16-Story	ELF	Pass	Pass	(5) Fail 16%	(3) Fail 3%
	RSA	Pass	Pass	(8) Fail 25%	(3) Fail 3%

some failures in the NDP; all the frames have a brace failure except the 4-story ELF-designed frame. If the median results are examined in lieu of the mean results, only the 8-story frames have brace failures.

When calculating the results for the NDP, consideration should be given to what values are used to determine the statistics (e.g., the mean and median values). Take, for example, two adjacent diagonal BRBs. The approach taken herein is to use the larger of the tension and compression  $DCR_N$  for a single brace for each ground motion, then calculate the mean or median for the record set based on this larger value. Next, the maximum of the left and right brace is reported for that floor. However, tension and compression damage states can be different. It may be useful to keep these actions separate and to calculate the statistics based on either the compression or the tension  $DCR_N$  for a single brace for each record, and then take the maximum of compression or tension as the controlling  $DCR_N$  for the record set. This approach would keep tension and compression separate and may provide different results than the envelope approach.

Another point to note is that both approaches are direction dependent. That is, if a ground motion is applied in the reverse direction, the numbers change. The direction the ground motions are applied is arbitrary. To remove this direction dependence, one could apply each earthquake in the positive and negative directions and calculate the desired statistic from these results. However, this would, in effect, statistically equate to the number of records used being doubled.

The distribution of brace failures illustrates how design choices can affect frame performance. In the 8-story frames, the  $DCR_N$  values are

the largest at the mid-height of the frames, indicating higher modes of vibration are influencing the behavior. Though it may be expected that the RSA-designed frame would perform better in this case, the results suggest otherwise. This may indicate that the magnitude of the design base shear is more important than the design force distribution (note: ASCE 7-16 [22] has changed the minimum design base shear for RSA to 100% of the ELF base shear). In comparison, the NSP results show the same general trend, but the magnitude of the  $DCR_N$  values are approximately half of those in the NDP. As was found in related research on special concentrically braced frames and eccentrically braced frames [6,7], the ground motion selection and scaling methodology employed in this research tends to exacerbate weakness in the frame designs. As such, the NDP gives some of the most conservative results when compared to the three other procedures investigated. Further details of the 8-story BRBF response are explored later in this section.

Table 7 also provides a summary of the performance of the column hinges for each nonlinear assessment procedure. In general, column hinges satisfy the performance criteria for both nonlinear procedures. However, base column hinges at the exterior of the frames consistently fail the performance criteria. These failures are a consequence of the column-to-base connection assumptions adopted for analysis and the modeling parameters for  $P$ - $M$  hinges in ASCE 41. The column members that fail the criteria are generally force-controlled for both axial force and flexure due to the axial load,  $P$ , exceeding 50% of the lower bound axial capacity,  $P_{CL}$ , for the NSP and NDP. The maximum axial force demand is from an individual record and, therefore, the determination of the force vs. deformation-controlled condition is biased by the behavior of the frame subject to one record even though other records may not result in  $P > 0.5 P_{CL}$ . Thus, it is difficult to capture record-to-record variability on force- and deformation-controlled responses directly in the analysis for a set of ground motion records. Another challenge with assessing column behavior using ASCE 41 is that the in-plane column hinge model and performance metrics are sometimes a function of the out-of-plane flexural buckling strength. This can be problematic because the relationship between in-plane hinging and out-of-plane buckling is not well-understood.

To probe further into the performance of the BRBF and understand why the 8-story braced frames have failures and why the nonlinear dynamic procedure produces the most conservative results of all the four procedures, the following issues are further explored: (1) ground motions selection and scaling, (2) conservatism in the linear assessment procedures, and (3) alternative assessment criteria.

**5.2.2.1. Issue 1: Ground motion selection and scaling.** The ground motion selection and scaling procedure may be one cause of the unsatisfactory results observed in the NDP assessment. The ground motions were selected from a set of 44 far-field records used in FEMA P695 [21]. This set was originally assembled with the intent of carrying out incremental dynamic analysis in which a building would be excited to a point of failure in order to determine the adequacy of system performance factors (i.e.,  $R$ ,  $\Omega_0$ , and  $C_d$ ) used in ASCE 7. The ground motions have many diverse characteristics that might not be reasonable for a building located at a specific geographic location. However, this set is assumed to be appropriate for use in this assessment given the intent of these archetype buildings to be generic in nature and not bound by any geographic location other than that assigned to SDC D.

To illustrate the results of sampling from the FEMA P695 set, the responses of the 8-story frames are investigated in more detail. Table 8 shows the details of the 14 selected ground motions and Tables 9 and 10 give a summary of the results ( $DCR_N$  values) using these ground motions. The tables give the median and maximum values for each story and which brace  $DCR_N$  values are controlled by tension or compression. Unlike results observed in a counterpart special concentrically braced frame study [6], there is no dominant trend between tension and compression failures. This is not surprising given the BRB's nearly symmetric tension and compression behavior.

**Table 8**  
Ground motion records used in the 8-story BRBF NDP.

ID	FEMA No.	Event Name	Station	Horizontal Component	Scale factor	Step (s)	Length (s)
EQ 1	3	Northridge	WLC	1	2.21	0.01	20
EQ 2	5	Duzce, Turkey	Bolu	1	2.02	0.01	56
EQ 3	10	Imperial Valley	Delta	2	2.43	0.01	100
EQ 4	12	Imperial Valley	El Centro Arr. #11	2	4.06	0.005	40
EQ 5	15	Kobe, Japan	Shin-Osaka	1	3.03	0.01	41
EQ 6	17	Kocaeli, Turkey	Duzce	1	2.43	0.005	28
EQ 7	20	Kocaeli, Turkey	Arcelik	2	5.75	0.005	30
EQ 8	22	Landers	Yermo Fire Station	2	4.47	0.02	44
EQ 9	28	Loma Prieta	Gilroy Array #3	2	2.07	0.005	40
EQ 10	31	Superstition Hills	El Centro Imp. Co.	1	2.82	0.005	40
EQ 11	34	Superstition Hills	Poe Road	2	2.97	0.01	23
EQ 12	38	Chi-Chi, Taiwan	CHY101	2	1.17	0.005	90
EQ 13	39	Chi-Chi, Taiwan	TCU045	1	4.86	0.005	90
EQ 14	42	San Fernando	LA - Hollywood	2	8.01	0.01	28

Select earthquake response spectra for the 8-story frames are shown in comparison to the  $MCE_R$  in Fig. 12. For the ELF-designed frame, EQs 4, 5, and 8 produce mid-to-lower story  $DCR_N$  values for the BRBs near the median for the suite (as indicated in Table 9). EQs 4, 5, and 8 have spectral accelerations at  $T_1$  (i.e., 2.06 s) of 1.10, 0.86, 1.16 times the  $MCE_R$  value, respectively. Additionally, the building period elongates once inelastic hinging occurs. As  $T_1$  increases, the response spectra values continue to be generally in the range of the  $MCE_R$ . EQ 13 produces the maximum mid-to-lower story  $DCR_N$  values for the suite. At  $T_1$  the spectral acceleration is 1.22 times the  $MCE_R$  value. As the building period increases, the response spectrum for EQ 13 is also generally in the range of the  $MCE_R$ , therefore it appears period elongation is not a significant concern for this case.

The RSA-designed frame performs worse than the ELF-designed frame. The maximum BRB  $DCR_N$  value occurs in the 4th story, where EQs 10 and 12 establish the median. EQs 6 and 13 help establish the median  $DCR_N$  values for several other stories. EQs 6, 10, 12, and 13 have spectral accelerations at  $T_1$  (i.e., 2.35 s) of 1.69, 1.17, 1.44, and 1.11 times the  $MCE_R$  value, respectively. The mean of the 14 spectral accelerations at  $T_1$  is 1.25 times the  $MCE_R$  value, which is due to scaling up the average of the record set such that it meets or exceeds the  $MCE_R$  over the range of  $0.2 T_1$ – $1.5 T_1$ .

EQ 3 establishes the maximum  $DCR_N$  values for the BRBs over the entire height of the frame (except 1st story) and is one of the three earthquakes that cause convergence problems in the analysis (the two

other earthquakes are EQ 7 and EQ 13). Based on inspection of the response spectrum, it is not immediately clear why EQ 3 produces the maximum building response; period elongation does not appear to be a problem since the response spectrum is well matched to the  $MCE_R$ . In general, long duration shaking (the scaled EQ 3 has a 0.05 g bracketed duration of 87 s) can be problematic, especially when the earthquake causes one-sided ratcheting driven by large P-Δ effects [23]. Fig. 13(b) shows the response of the roof-to-base drift with and without large P-Δ effects. As indicated, yielding of the braces in the middle stories starts at 7.1 s and all floors yield by 7.5 s. At 25 s, the 4th and 5th story braces reach their CP allowable deformation and by 44 s all braces at all floors reach their CP allowable deformations. From the point of yielding through the CP allowable deformation levels, the frame continues to ratchet over, in which the response can be qualified as being in a state of neutral equilibrium. At about 72 s the 1st story column hinges lose strength and a full collapse mechanism forms. Rigid body motion of the frame closely follows resulting in non-convergence of the solution algorithm.

In addition to issues with period elongation and ground motion duration, the influence of higher-mode response can also contribute to poor performance. The spectral compatibility between the selected records and the target spectrum is poor for periods less than approximately  $0.7 \times T_1$ , indicating higher modes are being excited above levels required in the design process. Researchers have pointed out that typically it is unrealistic for a ground motion spectrum to reach  $MCE_R$

**Table 9**  
 $DCR_N$  for the 8-story ELF-designed frame for the 14 earthquake records and the associated means and medians.

Story		EQ 1	EQ 2	EQ 3	EQ 4	EQ 5	EQ 6	EQ 7	EQ 8	EQ 9	EQ 10	EQ 11	EQ 12	EQ 13	EQ 14	Median	Mean
8	L	0.58	0.78	<u>2.00</u>	0.66	0.84	0.81	0.62	1.03	0.68	0.58	0.73	0.66	0.71	1.38	0.72	0.86
	R	0.58	0.78	<u>2.02</u>	0.66	0.84	0.82	0.59	1.03	0.67	0.58	0.72	0.67	0.74	1.37	0.73	0.86
7	L	0.62	<u>0.57</u>	1.76	0.54	0.90	<u>0.75</u>	0.66	0.77	0.39	0.35	0.65	0.49	0.84	1.41	0.65	0.76
	R	<u>0.62</u>	0.58	<u>1.78</u>	0.55	0.90	0.76	0.62	0.79	0.38	0.35	0.65	0.50	0.87	1.39	0.63	0.77
6	L	<u>0.57</u>	0.33	1.62	0.61	<u>0.90</u>	0.74	0.74	0.87	0.37	0.35	0.54	0.47	1.13	1.56	0.67	0.77
	R	0.57	<u>0.34</u>	<u>1.64</u>	0.60	0.89	<u>0.76</u>	0.75	0.86	0.38	0.36	0.53	0.47	1.17	1.53	0.68	0.77
5	L	0.71	0.37	1.66	0.89	<u>1.02</u>	<u>0.97</u>	1.14	0.99	0.51	0.64	0.62	0.71	1.80	1.78	0.93	0.99
	R	<u>0.71</u>	0.37	1.67	0.88	<u>1.01</u>	0.99	1.19	<u>0.98</u>	0.52	0.65	0.61	0.71	<u>1.84</u>	1.75	0.93	0.99
4	L	<u>0.90</u>	<u>0.45</u>	1.72	1.07	<u>1.16</u>	<u>1.25</u>	1.61	1.22	0.60	0.87	0.82	0.92	2.20	1.90	1.12	1.19
	R	0.91	0.44	1.72	1.06	<u>1.15</u>	<u>1.25</u>	1.58	1.22	0.61	0.87	0.82	0.92	<u>2.21</u>	<u>1.91</u>	1.10	1.19
3	L	0.97	<u>0.60</u>	1.65	1.25	1.32	<u>1.51</u>	2.04	1.27	0.70	1.07	0.95	1.10	2.46	1.94	1.26	1.34
	R	<u>0.98</u>	<u>0.58</u>	1.65	1.23	1.30	1.50	<u>2.02</u>	1.26	0.70	1.08	0.96	1.09	<u>2.47</u>	1.95	1.24	1.34
2	L	<u>0.92</u>	0.68	1.51	1.40	1.42	<u>1.60</u>	2.28	1.17	0.71	1.12	0.98	1.07	2.56	1.83	1.28	1.37
	R	<u>0.94</u>	<u>0.72</u>	1.52	1.40	<u>1.41</u>	1.63	2.32	1.18	0.70	1.12	0.96	1.09	<u>2.67</u>	<u>1.80</u>	1.29	1.39
1	L	<u>0.75</u>	0.56	1.26	1.29	<u>1.24</u>	<u>1.42</u>	2.37	0.87	0.53	0.92	0.78	0.77	<u>1.38</u>	<u>1.55</u>	1.08	1.84
	R	0.77	0.59	1.25	1.30	<u>1.25</u>	1.44	2.39	0.88	0.53	0.92	0.77	0.79	<u>2.63</u>	1.52	1.08	1.22

Notes: L = left brace; R = right brace; EQ = earthquake; underlined = tension governed  $DCR_N$ ; shading = value(s) that established controlling median; “boxed” value = maximum for each story

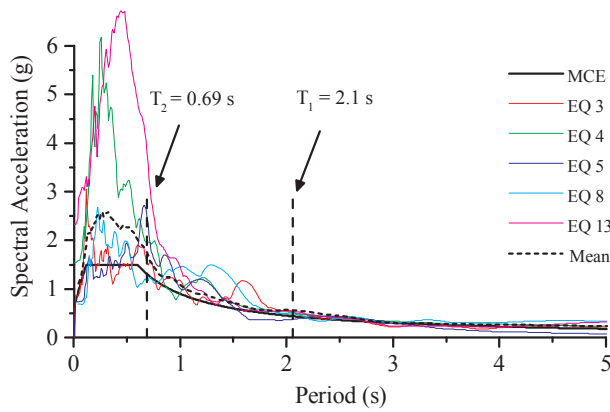
Notes: L = left brace; R = right brace; EQ = earthquake; underlined = tension governed  $DCR_N$ ; shading = value(s) that established controlling median; “boxed” value = maximum for each story.

**Table 10**  
 $DCR_N$  for the 8-story RSA-designed frame for the 14 earthquake records and the associated means and medians.

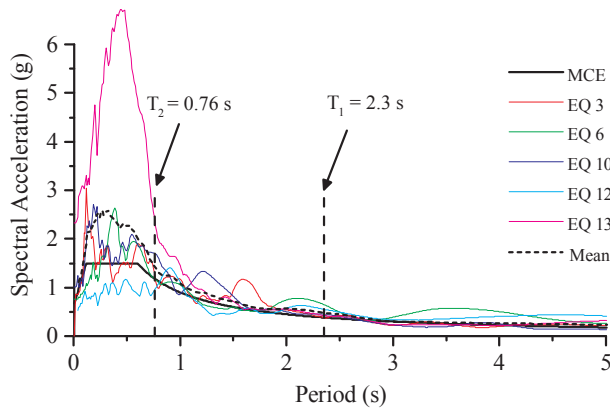
Story		EQ 1	EQ 2	EQ 3	EQ 4	EQ 5	EQ 6	EQ 7	EQ 8	EQ 9	EQ 10	EQ 11	EQ 12	EQ 13	EQ 14	Median	Mean
8	L	<u>0.38</u>	0.37	<u>1.77</u>	0.67	0.57	<u>0.45</u>	0.34	<u>1.39</u>	0.30	0.32	0.37	<u>0.34</u>	<u>0.35</u>	0.86	0.38	0.61
	R	0.38	0.37	1.79	0.63	0.56	0.48	0.34	1.43	<u>0.30</u>	<u>0.32</u>	<u>0.37</u>	0.36	0.35	<u>0.84</u>	0.38	0.61
7	L	0.52	0.30	<u>1.99</u>	<u>1.16</u>	<u>0.80</u>	0.61	0.41	1.84	0.30	0.46	<u>0.39</u>	0.76	<u>0.59</u>	<u>1.31</u>	0.60	0.82
	R	<u>0.53</u>	<u>0.31</u>	<u>2.02</u>	1.14	0.79	<u>0.63</u>	0.43	<u>1.88</u>	<u>0.30</u>	<u>0.47</u>	0.38	<u>0.78</u>	<u>0.64</u>	1.29	0.64	0.83
6	L	<u>0.78</u>	<u>0.42</u>	<u>2.60</u>	1.85	1.12	<u>0.85</u>	<u>1.21</u>	<u>2.45</u>	<u>0.59</u>	<u>0.83</u>	0.74	<u>1.27</u>	<u>1.00</u>	1.86	1.06	1.25
	R	0.79	0.43	2.64	1.82	1.11	0.88	1.29	2.47	0.60	0.85	<u>0.73</u>	1.31	1.05	<u>1.82</u>	1.08	1.27
5	L	1.07	0.59	<u>3.33</u>	<u>2.55</u>	<u>1.37</u>	1.21	2.14	2.87	0.83	1.35	<u>1.00</u>	1.76	1.48	<u>2.21</u>	1.43	1.70
	R	<u>1.09</u>	<u>0.60</u>	<u>3.37</u>	2.52	1.37	1.25	2.23	<u>2.89</u>	<u>0.83</u>	<u>1.37</u>	0.99	1.79	<u>1.55</u>	2.17	1.46	1.71
4	L	<u>1.18</u>	<u>0.69</u>	<u>3.62</u>	2.87	1.41	<u>1.41</u>	<u>2.69</u>	<u>2.89</u>	<u>0.85</u>	<u>1.72</u>	1.12	<u>1.96</u>	<u>2.08</u>	2.14	1.84	1.90
	R	1.20	0.71	3.64	2.86	1.40	1.45	2.76	2.90	0.85	1.73	<u>1.11</u>	<u>1.98</u>	2.12	<u>2.09</u>	1.85	1.91
3	L	1.23	0.82	<u>3.56</u>	<u>2.87</u>	<u>1.39</u>	1.47	2.87	2.57	0.84	1.83	<u>1.09</u>	1.87	2.59	<u>1.75</u>	1.79	1.91
	R	<u>1.26</u>	<u>0.85</u>	<u>3.58</u>	2.85	1.37	<u>1.52</u>	<u>2.94</u>	<u>2.59</u>	<u>0.85</u>	<u>1.84</u>	1.08	<u>1.89</u>	<u>2.66</u>	<u>1.70</u>	1.77	1.93
2	L	<u>1.07</u>	<u>0.78</u>	<u>3.23</u>	2.54	1.29	<u>1.41</u>	<u>2.86</u>	<u>2.19</u>	<u>0.73</u>	<u>1.64</u>	0.98	<u>1.66</u>	<u>2.79</u>	1.28	1.52	1.75
	R	1.06	0.78	3.23	<u>2.55</u>	<u>1.29</u>	1.39	2.83	2.19	0.73	1.63	<u>0.99</u>	1.65	3.16	<u>1.29</u>	1.51	1.77
1	L	0.71	0.58	10.35	<u>2.00</u>	<u>0.99</u>	1.01	2.78	1.65	0.50	1.16	<u>0.69</u>	1.20	<u>10.88</u>	<u>0.79</u>	1.09	2.52
	R	0.71	0.58	2.81	2.04	1.00	0.99	2.66	1.61	0.49	1.14	0.70	1.18	3.06	0.81	1.07	1.41

Notes: L = left brace; R = right brace; EQ = earthquake; underlined = tension governed  $DCR_N$ ; shading = value(s) that established controlling median; “boxed” value = maximum for each story

Notes: L = left brace; R = right brace; EQ = earthquake; underlined = tension governed  $DCR_N$ ; shading = value(s) that established controlling median; “boxed” value = maximum for each story



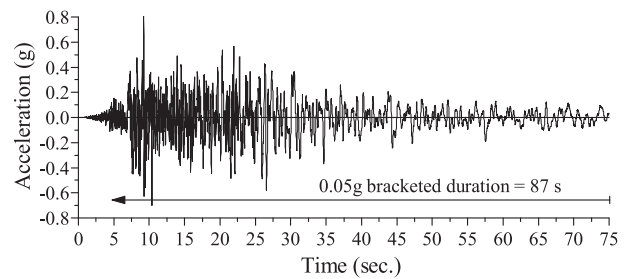
a) ELF-designed frame



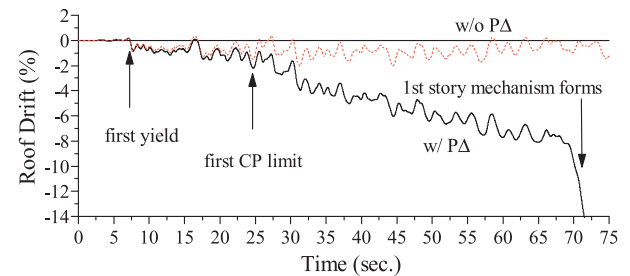
b) RSA-designed frame

**Fig. 12.** Response spectra for the earthquakes that produce values near the median and the earthquake that produces the maximum for (a) the ELF-designed frame and (b) the RSA-designed frame.

levels at both the first and second mode of a building [24]; the difference in shape between rare earthquakes and more frequently occurring earthquakes indicates that rare earthquakes tend to have a spectral peak at the period of interest. The consequence is that when one considers and properly accounts for the spectral shape in the selection and scaling process, the collapse margin ratio can increase substantially:



(a)



(b)

**Fig. 13.** (a) The scaled EQ 3 ground motion acceleration record and (b) the roof drift (relative to the ground) of 8-story RSA-designed frame subjected to EQ 3 with and without large P-Δ.

40–60% reported by FEMA P695 and Haselton et al. [25].

Analogous to the consideration of spectral shape are the problems associated with amplitude scaling of input ground motions. In this study, no limit is placed on the maximum scale factor and all records are scaled up for the BSE-2N scenario, with scale factors ranging from 1.1 to 8.0 (see Table 8). The scale factor for EQ 3 for the 8-story ELF designed frame is 2.4, which is towards the lower end of scale factors that are used herein. Regardless, upwards scaling can be indicative of either a ground motion having a spectral shape with a “valley”, or relative low point, at the period of interest (i.e.,  $T_1$ ) or a ground motion coming from a relatively more frequent, less intense event. Luco and Bazzurro [26] demonstrated that structural response tends to be conservatively biased for records that have upwards scaling. Amplitude scaling is an unavoidable consequence of having limited strong ground motion records.

To supplement the results presented herein, different ground motion selection and scaling approaches should be investigated to determine their effect on the assessment results. These approaches could include selecting from a larger database of records and/or using emerging methodologies such as the site-specific conditional mean spectrum approach developed by Baker [27]. Uribe et al. [28] showed that using the conditional mean spectrum approach significantly improves the results and provides a lower level of dispersion, which can be an indication of reduced uncertainty. Other research has shown that record selection methods that control the mismatch between the target spectrum and each record spectrum can also improve the robustness of the mean response estimate [29]. Each of these alternative approaches should be weighed in terms of cost and efficiency.

**5.2.2.2. Issue 2: adequacy of the linear procedures.** The challenges of capturing highly nonlinear response with a linear modeling approach are well established. Linear analysis is not able to capture the effects of period elongation as the structure yields, nor the effects of ductility demand concentration due to the formation of a story mechanism. Therefore, it is difficult to draw too many definitive conclusions from the linear analysis when the structure is expected to perform in a highly nonlinear fashion, as noted in ASCE 41. Regardless, the fact that the linear assessment procedures produced less conservative results compared to the nonlinear procedures is a concern, since generally the opposite is expected. To further understand the building performance, the probability of collapse (given a maximum considered earthquake) should be determined via a FEMA P695 analysis to see if the design is meeting the intent of ASCE 7.

**5.2.2.3. Issue 3: Assessment criteria - maximum demand vs. cumulative demand.** For all component types, ASCE 41 uses a maximum permissible deformation as the metric for determining acceptance. Though this seems reasonable, it is indifferent to the demand history a component has been subjected. In other words, the permissible deformation does not change based on how much energy has been dissipated in a plastic manner. Fundamental material behavior suggests that a BRB's deformation capacity is dependent on the loading history. ASCE 41 takes the simplistic approach of using a first-cycle backbone curve based on the fully-reversed cyclic loading protocol. If the true loading history during an earthquake is one-sided or monotonic, the permissible deformations may be too conservative [30]. Therefore, it is recommended that the maximum deformation-type acceptance criteria listed in ASCE 41 Table 9-7 be re-examined.

For example, a methodology based on cumulative ductility could be implemented. AISC 341-10 requires qualification testing to demonstrate each brace has a cumulative inelastic axial deformation capacity of 200 times the yield deformation. To account for the cumulative effects, the permissible deformations listed in ASCE 41 Table 9-7 could be multiplied by an adjustment factor,  $\mu_a$ , defined as:

$$\mu_a = a - b(\mu_c/200) \tag{9}$$

where  $\mu_c$  is the cumulative ductility demand and coefficients  $a$  and  $b$  determine the multiplier on the permissible deformation given a monotonic loading and the relative importance of the cumulative ductility reduction, respectively. The cumulative ductility demand is defined in [31] as:

$$\mu_c = \sum \frac{\Delta_{plastic}}{\Delta_{by}} \tag{10}$$

where  $\Delta_{plastic}$  is the BRB plastic deformation and  $\Delta_{by}$  is the BRB yield deformation, and the summation is over all deformation cycles.

Coefficients  $a$  and  $b$  should be calibrated using test data to ensure both monotonic and fully-reversed cyclic loading history behaviors are captured in a reasonable manner. Given a loading history that is monotonic, the permissible deformations would be essentially

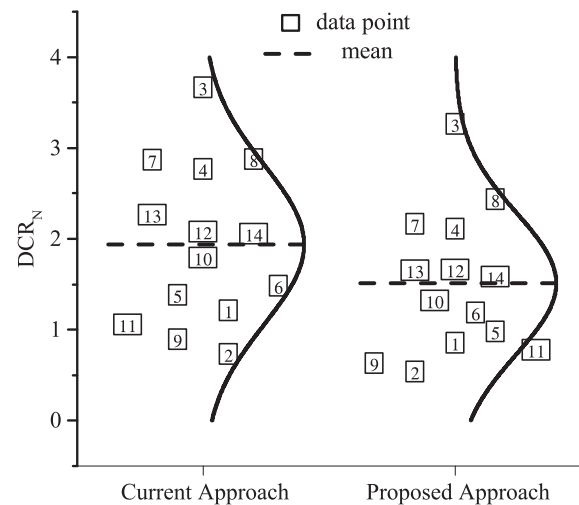


Fig. 14. Effects of using the proposed permissible deformation adjustment factor for the 4th story brace in the 8-story RSA-designed frame (boxed number signifies earthquake).

multiplied by  $a$ . Researchers have shown that BRBs can reach deformations of  $20 \times \Delta_{by}$  or greater [31]. In contrast, ASCE 41 CP permissible inelastic deformation is  $13.3 \times \Delta_{by}$ , therefore the effective increase of the permissible deformations may be warranted (e.g.,  $a = 1.5$ ).

As an example of the potential effects of implementing Eq. (9), let  $a = 1.5$  and  $b = 0.5$  and then recalculate the assessment results for the 4th story brace in the 8-story RSA-designed frame. The cumulative deformation demand is calculated for each earthquake simulation and then Eq. (9) is used to calculate the adjustment factor. The current versus proposed  $DCR_N$  values for each simulation are presented in Fig. 14. The mean cumulative deformation demand is 73 with a standard deviation of 36. The maximum cumulative deformation demand is recorded from EQ 3, with a value of 151. For this case the adjustment factor is 1.13, therefore the  $DCR_N$  value goes from 3.64 to 3.22—a 10% reduction. For the entire suite, the adjustment factors range from 1.13 to 1.42. The net result for this example shifts the mean and median  $DCR_N$  down from 1.91 to 1.49 and 1.85 to 1.41, respectively—a 20% reduction. Similar calculations can be made for the rest of the braces. Eq. (9) is presented as an example to spur further development; more investigation on this topic is warranted, which could include energy-based “damage index” approaches investigated by other researchers [32–34].

## 6. Summary and conclusions

The ASCE 41 seismic performance assessment for a suite of six BRBFs can result in varying performance outcomes. The ASCE 41 procedures generally suggest the 4- and 16-story frames have satisfactory performance except for yielding of the base columns. In contrast, the performance of the 8-story frames is deficient per the ASCE 41 procedures. The nonlinear dynamic procedure produces particularly conservative results (relative to the linear procedures), which contradicts the typical understanding that an analysis of increased rigor will give less conservative results. These results expose the need for clarification and/or refinement of certain provisions in ASCE 41. A building with seemingly reasonable strength distribution and ductility (as provided by ASCE 7) is seen to be vulnerable to unsatisfactory nonlinear performance, which went undetected during the linear design and assessment process. The resulting brace failures in the nonlinear dynamic procedure are reasonably distributed along the height of the frame, suggesting member proportioning is not the root cause of the performance deficiencies. High demands imparted by certain ground motions result in numerous braces yielding simultaneously. The yielding spreads

from the mid-height of the frame to the base and eventually a story mechanism is formed when the base columns experience significant flexural yielding. Challenges associated with selection and scaling of ground motions also contribute to the nonlinear dynamic assessment results, though the median values seem to be governed by ground motions with spectral shapes within a reasonable scatter from the  $MCE_R$  spectrum. Similar observations are made in companion papers investigating the performance of special concentrically braced frames [6] and eccentrically braced frames [7]. Additionally, the inability of the performance assessment criteria to account for cumulative deformation effects is discussed, and an adjustment to the permissible deformation limits is proposed.

In closing, the following conclusions and recommendations can be made:

1. Linear assessment procedures tend to give less conservative results than those determined from their counterpart nonlinear procedures for the buildings and models employed. Based on the work presented here, it is unclear whether the linear assessment results are in fact unconservative or the nonlinear assessment results are overly conservative. To further probe this issue, the building's probability of collapse (given a maximum considered earthquake) should be determined via a FEMA P695 analysis to benchmark the performance relative to the design intent of ASCE 7.
2. It is expected that the process used for the selection and scaling of ground motions has an impact on the assessment results using the NDP. Since there is a limited number of strong motion records with spectral accelerations close to those needed to represent the  $MCE_R$ , other selection and scaling procedures should be investigated. For example, site-specific approaches, such as the conditional mean spectrum, can be implemented for known building sites.
3. ASCE 41 could consider the use of assessment criteria that accounts for loading history. Use of an adjustment factor based on cumulative inelastic deformation is one viable option. The approach suggested herein reduces the relative conservatism of the nonlinear dynamic assessment results.
4. About developing a link between ASCE 7 and ASCE 41, the primary difficulty in equating the two standards is rooted in their dissimilar performance objectives. Acceptance criteria for a component in ASCE 41 are not directly calibrated to the seismic performance objective of ASCE 7. Results from this study indicate that for ASCE 41 to be used as an alternative to ASCE 7, acceptance criteria for the various analysis methods must be calibrated relative to each other if uniform risk is desired.

## 7. Disclaimer

Certain commercial software, equipment, instruments, or materials may have been used in the preparation of information contributing to this paper. Identification in this paper is not intended to imply recommendation or endorsement by NIST, nor is it intended to imply that such software, equipment, instruments, or materials are necessarily the best available for the purpose.

## References

- [1] ASCE. Minimum Design Loads for Buildings and Other Structures. ASCE/SEI 7-10. Reston, VA: American Society of Civil Engineers; 2010.
- [2] ASCE. Seismic Rehabilitation of Existing Buildings. ASCE/SEI 41-06. Reston, VA: American Society of Civil Engineers; 2006.
- [3] NIST. Research Required to Support Full Implementation of Performance-Based Seismic Design. NIST GCR 09-917-2: Prepared by the Building Seismic Safety Council of the National Institute of Building Sciences; 2009.
- [4] Adams S. Performance-Based Analysis of Steel Buildings: Special Concentric Braced Frame: California Polytechnic State University; 2010.
- [5] Burkholder M. Performance-Based Analysis of a Steel Braced Frame Building with Buckling Restrained Braces: California Polytechnic State University; 2012.
- [6] Speicher MS, Harris JL. Collapse prevention seismic performance assessment of new special concentrically braced frames using ASCE 41. *Eng Struct* 2016;126:652–66.
- [7] Speicher MS, Harris JL. Collapse prevention seismic performance assessment of new eccentrically braced frames using ASCE 41. *Eng Struct* 2016;117:344–57.
- [8] Harris JL, Speicher MS. Assessment of First Generation Performance-Based Seismic Design Methods for New Steel Buildings, Volume 1: Special Moment Frames. Gaithersburg, MD: National Institute of Standards and Technology; 2015. <https://doi.org/10.6028/NIST.TN.1863-1>.
- [9] Speicher MS, Harris JL. ASCE/SEI Predicted Performance of Newly Designed BRBFs. 16th World Conference on Earthquake Engineering. Santiago, Chile 2017.
- [10] Harris JL, Speicher MS. Assessment of First Generation Performance-Based Seismic Design Methods for New Steel Buildings, Volume 2: Special Concentrically Braced Frames. Gaithersburg, MD: National Institute of Standards and Technology; 2015. <http://dx.doi.org/10.6028/NIST.TN.1863-2>.
- [11] Harris JL, Speicher MS. Assessment of First Generation Performance-Based Seismic Design Methods for New Steel Buildings, Volume 3: Eccentrically Braced Frames. Gaithersburg, MD: National Institute of Standards and Technology; 2015. <http://dx.doi.org/10.6028/NIST.TN.1863-3>.
- [12] ICC. International Building Code (IBC). Washington, DC: International Code Council; 2012.
- [13] AISC. Seismic Provisions for Structural Steel Buildings. ANSI/AISC 341-10. Chicago, IL: American Institute of Steel Construction; 2010.
- [14] Speicher MS, Harris JL. Assessment of First Generation Performance-Based Seismic Design Methods for New Steel Buildings, Volume 4: Buckling-Restrained Braced Frames. Gaithersburg, MD: National Institute of Standards and Technology; Under Review.
- [15] Thornton WA, Muir LS. Vertical Bracing Connections in the Seismic Regime. In: AISC, editor. Connections VI: Sixth International Workshop on Connections in Steel Structures. Chicago, IL: AISC; 2008.
- [16] CSI. Extended Three Dimensional Analysis of Building Systems. ETABS. Version 9.7. 4 ed. Berkeley, CA: Computers and Structures, Inc.; 2013.
- [17] CSI. Nonlinear Analysis and Performance Assessment for 3D Structures. PERFORM 3D. Version 5.0 ed. Berkeley, CA: Computers and Structures, Inc.; 2013.
- [18] Merritt S, Uang C-M, Benzoni G. Subassemblage testing of star seismic buckling-restrained braces. San Diego: University of California; 2003.
- [19] Newell J, Uang C-M, Benzoni G. Subassemblage testing of corebrace buckling-restrained braces (G Series). San Diego: University of California; 2006.
- [20] CSI. Components and Elements for PERFORM-3D and PERFORM-COLLAPSE. Berkeley, CA: Computers and Structures, Inc.; 2011.
- [21] FEMA. Quantification of Building Seismic Performance Factors. FEMA P695. Washington, D.C.: Department of Homeland Security; 2009.
- [22] ASCE. Minimum Design Loads for Buildings and Other Structures. ASCE/SEI 7-16: American Society of Civil Engineers; 2017.
- [23] Chandramohan R, Baker JW, Deierlein GG. Quantifying the influence of ground motion duration on structural collapse capacity using spectrally equivalent records. *Earthquake Spectra* 2016;32:927–50.
- [24] Baker JW, Cornell CA. Spectral shape, epsilon and record selection. *Earthquake Eng Struct Dyn* 2006;35:1077–95.
- [25] Haselton CB, Baker JW, Liel AB, Deierlein GG. Accounting for ground-motion spectral shape characteristics in structural collapse assessment through an adjustment for epsilon. *J Struct Eng* 2011;137:332–44.
- [26] Luco N, Bazzurro P. Does amplitude scaling of ground motion records result in biased nonlinear structural drift responses? *Earthquake Eng Struct Dyn* 2007;36:1813–35.
- [27] Baker JW. Conditional mean spectrum: tool for ground-motion selection. *J Struct Eng* 2011;137:322–31.
- [28] Uribe R, Sattar S, Speicher MS, Ibarra L. Influence of Ground Motion Selection on the Assessment of a Steel Special Moment Frame. 16th World Conference on Earthquake Engineering. Santiago, Chile 2017.
- [29] Araujo M, Macedo L, Marques M, Castro JM. Code-based record selection methods for seismic performance assessment of buildings. *Earthquake Eng Struct Dyn* 2016;45:129–48.
- [30] Maison BF, Speicher MS. Loading protocols for ASCE 41 backbone curves. *Earthquake Spectra* 2016;32:1–20.
- [31] Fahnstock LA, Sause R, Ricles JM. Seismic response and performance of buckling-restrained braced frames. *J Struct Eng* 2007;133:1195–204.
- [32] Johnson JG, Pantelides CP, Reveley LD. Nonlinear rooftop tuned mass damper frame for the seismic retrofit of buildings. *Earthquake Eng Struct Dyn* 2015;44:299–316.
- [33] Park YJ, Ang AHS, Wen YK. Seismic damage analysis of reinforced concrete buildings. *J Struct Eng* 1985;111:740–57.
- [34] Fardis MN. Damage measures and failure criteria for reinforced concrete members. Proceedings of the 1994 10th European Conference on Earthquake Engineering Vol 2 (of 4), Aug 28 - Sep 2 1994. Vienna, Austria 1995. p. 1377.